Implementation of the Quasi-equilibrium Tropical Circulation Model 2 (QTCM2): Global simulations and convection sensitivity to free tropospheric moisture

Benjamin R. Lintner,[1] Gilles Bellon,[2] Adam H. Sobel,[3,4,5] Daehyun Kim,[3] and J. David Neelin[6]

[1] The implementation of the Quasi-equilibrium Tropical Circulation Model 2 (QTCM2), an intermediate level complexity model, is described. Following the approach of Sobel and Neelin (2006), an explicit, prognostic atmospheric boundary layer (ABL) of fixed depth is added to a free troposphere (FT) containing one baroclinic and one barotropic mode. QTCM2 is shown to simulate reasonable climatologies of temperature, moisture, winds, and precipitation, albeit with only modest improvements relative to the predecessor single vertical mode version, QTCM1. The addition of an ABL increases the sharpness of horizontal precipitation and moisture gradients, and the separation of the moisture profile into ABL and FT components allows investigation into the separate roles of these two components in modulating deep convection. Model sensitivity to various convection parameters is explored, with contrasting precipitation responses often seen within the cores of convecting regions and along their margins.

1. Introduction

[2] Quasi-equilibrium Tropical Circulation Models (QTCMs) are a family of intermediate level complexity models employing a Galerkin-like vertical discretization in which the primitive equations are projected onto a few prescribed, physically-based, vertical structure functions [*Neelin and Zeng*, 2000]. For large-scale tropical motions, the term convective quasi-equilibrium (QE) refers to the idea that deep convection constrains the vertical structure of temperature and moisture to lie close to known statistical equilibrium profiles in convecting regions. Efficient equatorial wave dynamics communicates the temperature structure laterally throughout the Tropics. For a given temperature basis function and assuming hydrostatic balance, basis functions for velocity are constructed to be consistent with the implied vertical structures of baroclinic and barotropic pressure gradients. The first QTCM, hereafter QTCM1, comprises a single first baroclinic mode in temperature and barotropic and first baroclinic modes in momentum [*Zeng et al.*, 2000].

[3] In contrast to many other idealized models, QTCM1 retains nonlinearities inherent to the primitive equations and further incorporates parameterizations resembling those found in general circulation models (GCMs). For example, the radiative scheme implemented in QTCM1 was derived from a linearized radiative transfer scheme [*Chou and Neelin*, 1996] and includes cloud-radiative feedbacks for different cloud types. Apart from QTCM1's computational efficiency, one of the more useful aspects of the model is the ease of diagnosis of tropical moist dynamics. Among the diverse phenomena previously studied with QTCM1 are: tropical land and ocean region precipitation climatology and variability [*Zeng et al.*, 2000]; remote tropical ENSO teleconnections [*Chiang and Sobel*, 2002; *Neelin and Su*, 2005; *Lintner and Chiang*, 2007]; global warming impacts on tropical precipitation [*Neelin et al.*, 2003; *Chou and Neelin*, 2004]; midlatitude transient effects on tropical precipitation variability [*Lin et al.*, 2000]; and theories for monsoon structure and spatial characteristics in current and past climates [*Chou and Neelin*, 2003; *Su and Neelin*, 2005]. Moreover, the vertically-projected equations in QTCM1 have been used as a starting point

[1]Department of Environmental Sciences, Rutgers, State University of New Jersey, New Brunswick, New Jersey, USA.

[2]Centre National de Recherches Météorologiques, Centre National de la Recherche Scientifique, Météo-France, Toulouse, France.

[3]Department of Applied Physics and Applied Mathematics, Columbia University, New York, New York, USA.

[4]Department of Earth and Environmental Sciences, Columbia University, New York, New York, USA.

[5]Lamont-Doherty Earth Observatory, Columbia University, New York, New York, USA.

[6]Department of Atmospheric and Oceanic Sciences and Institute of Geophysics and Planetary Physics, University of California, Los Angeles, California, USA.

for analytic solutions for tropical circulations under the weak temperature gradient approximation [*Sobel and Bretherton*, 2000; *Sobel et al.*, 2001]; idealized models of Hadley and Walker circulations [*Bretherton and Sobel*, 2002; *Sobel et al.*, 2004; *Burns et al.*, 2006]; convectively coupled waves [*Khouider and Majda*, 2006; *Frierson*, 2007]; interactions of inflow air mass characteristics with tropical deep convection [*Lintner and Neelin*, 2007, 2008]; and land-atmosphere coupling [*Lintner et al.*, 2012]. Such analytical solutions often suggest relationships that are not obvious from diagnostics alone and facilitate the development of additional diagnostics for more complex models.

[4] While QTCM1 has yielded insights into a wide range of tropical phenomena, its limited vertical degrees of freedom preclude consideration of some fundamental aspects of tropical climate. One obvious limitation of QTCM1 is its lack of an explicit atmospheric boundary layer (ABL) independent of the free troposphere (FT). To address this limitation, Sobel and Neelin (2006, hereinafter SN06) developed a self-consistent, axisymmetric version of QTCM with separate thermodynamic and momentum equations for the ABL and FT. SN06 used their two-level QTCM, or QTCM2, to examine how thermodynamic and momentum controls contribute to the intensity and meridional extent of Intertropical Convergence Zones (ITCZs). They found that inclusion of an ABL in the axisymmetric configuration enhances both the amplitude and sharpness of ITCZs, consistent with boundary layer convergence acting as a forcing on the free troposphere (FT) [*Lindzen and Nigam*, 1987; *Back and Bretherton*, 2009]. *Bellon and Sobel* [2010] used the axisymmetric model of SN06 to investigate equatorial symmetry-breaking mechanisms and the occurrence of multiple equilibria for the Hadley circulation. This axisymmetric model was further used to study mechanisms of the monsoon intraseasonal oscillation [*Bellon and Sobel*, 2008a, 2008b], as well as its coupling with oceanic and continental surfaces [*Bellon et al.*, 2008; *Bellon*, 2011].

[5] The present study extends the axisymmetric QTCM2 of SN06 to a non-axisymmetric "2.5D" configuration with realistic boundary conditions. Following a brief discussion of the model's implementation (Section 2), we present an overview of QTCM2-simulated climatologies (Section 3). Section 4 highlights some aspects of QTCM2 sensitivity: in particular, we directly illustrate how independent ABL and FT thermodynamics and dynamics, the principal difference vis-à-vis QTCM1, impact precipitation simulation. We further demonstrate how the use of revised vertical structure functions and a modified convection scheme alter simulated precipitation.

[6] Beyond the model configuration sensitivity analyses in Section 4, we also investigate some aspects of convective sensitivity to FT moisture (Section 5). While observational and cloud system resolving model studies indicate that moist convection is sensitive to FT moisture [*Parsons et al.*, 2000; *Tompkins*, 2001; *Grabowski and Moncrieff*, 2004; *Bretherton et al.*, 2004; *Sherwood et al.*, 2004; *Derbyshire et al.*, 2004], global climate models (GCMs) often underestimate or otherwise fail

to reflect this sensitivity [*Biasutti et al.*, 2006; *Dai*, 2006]. The lack of sensitivity may stem from underestimation of entrainment and rain re-evaporation, so models produce deep convection too readily [*Kuang and Bretherton*, 2006; *Del Genio*, 2012]. At the same time, GCM studies provide evidence that the entrainment rate or other parameters impacting this convective moisture sensitivity have a substantial impact on many phenomena including intraseasonal variability such as the Madden Julian Oscillation (MJO) [*Grabowski*, 2006; *Kim et al.*, 2011; *Hannah and Maloney*, 2011], and that deficiencies in model representation of feedbacks between moisture, deep convection, and circulation may ultimately limit the ability of GCMs to simulate multiscale convective organization [*Holloway and Neelin*, 2010], particularly on intraseasonal scales. Although the analysis presented in Section 5 is cursory, we believe it illustrates QTCM2's utility as a tool for addressing some important features of convective sensitivity to FT moisture.

2. Model Implementation

[7] The implementation of the non-axisymmetric QTCM2 with realistic boundary conditions closely follows the implementation of the axisymmetric version described in SN06. Relative to QTCM1, these modifications fall into one of three categories: (i) *model physics*, associated with the added vertical degree of freedom; (ii) *model parameterization schemes*, revised as a result of separating the ABL and FT basis functions (but which are updated within the same overall physical framework); and (iii) *model parameters*, revised as a result of the updated vertical basis functions. We also note that several errors in the base code for QTCM1 (specifically, version 2.3) have been corrected, although the impacts of these on simulations performed with existing model versions are small. Below we highlight key features of QTCM2, noting specifically where the implementation diverges from either SN06 or the QTCM1v2.3 base code. The reader is referred to Appendix A for a more detailed review of the mathematical basis of QTCM2. QTCM2 source code and documentation can be found at: http://www.atmos.ucla.edu/~csi/QTCM/qtcm.html.

2.1. Momentum Equations Formulated in Vorticity-Divergence Form

[8] The major structural difference in the full non-axisymmetric implementation involves the ABL and barotropic velocity fields. (We use the term "barotropic" loosely here to refer to the vertically uniform component of the FT velocity; because the ABL velocity differs from that component, this mode is not strictly barotropic.) For the axisymmetric version of SN06, the column-integrated meridional momentum, a linear combination of the ABL and barotropic meridional winds, is identically zero, because of the axisymmetric continuity equation and the latitudinal boundary conditions. This allowed the use of meridional momentum budgets in the ABL and the FT to compute the gradient of surface geopotential and either the ABL or the barotropic meridional wind. In the present non-axisymmetric

implementation, this is not the case; rather, we use the vorticity-divergence (vort-div) form of the barotropic momentum equations. (The baroclinic momentum equations are solved in component form.) Consider the time-tendency of the (horizontal) barotropic momentum in the FT:

$$\partial_t \mathbf{v}_0 = \mathbf{F}_{\mathbf{v}0} \tag{1}$$

where $\mathbf{F}_{\mathbf{v}0}$ represents the sum of all barotropic momentum tendencies. Expanding the wind in divergent and rotational components $\mathbf{v}_0 = \mathbf{v}_\phi + \mathbf{v}_\psi = \nabla\phi + \nabla\times\psi\hat{\mathbf{k}}$, with ϕ the velocity potential and ψ the streamfunction, and evaluating the curl and divergence of equation (1) gives respectively:

$$\nabla^2 \partial_t(\phi,\psi) = (\nabla\cdot\mathbf{F}_{\mathbf{v}0}, \hat{\mathbf{k}}\cdot\nabla\times\mathbf{F}_{\mathbf{v}0}) \tag{2}$$

Equation (2) is of the form of a Poisson equation in the time-tendencies of the scalar variables ϕ and Ψ. Formally, an analogous equation applies to the ABL, although the divergent ABL and FT barotropic winds are related through mass conservation as in equation (A13). Fast-Fourier Transform Poisson solvers are applied to equation (2) as well as the ABL streamfunction equation to obtain the time-tendencies of ϕ and ψ, which are updated and then used to obtain the velocity fields.

2.2. Vertical Structure Coefficients

[9] The implementation of QTCM2 employs revised temperature, moisture, and first baroclinic momentum basis functions, $a_1(p)$, $b_1(p)$, and $V_1(p)$ in the FT portion of the domain as described in *Holloway and Neelin* [2007, 2009] (see Figure 1). Relative to the vertical profiles assumed in QTCM1, the revised temperature profile $a_1(p)$ includes a partial representation of the convective cold top, with the relative weighting decreasing in the upper troposphere above ~250 mb, while the revised moisture profile $b_1(p)$ implies lower values in the lower FT. Differences in the simulation of the cold top in aquaplanet GCMs appear to contribute to intermodel differences in ITCZ structure and ITCZ regime transitions

[*Oueslati and Bellon*, 2012]. In the ABL, the basis functions are assumed to be vertically uniform. Values of coefficients precomputed from these basis functions are summarized in Table 1.

[10] As discussed in SN06, gross stratifications are computed for both the FT barotropic and baroclinic modes; these are of the general form:

$$\begin{aligned} M_{si} &= M_{sri} + M_{spi}T_1 \\ M_{qi} &= M_{qri} + M_{qpi}q_1 \end{aligned} \tag{3}$$

where the index i is either 0 or 1. With the exception of the baroclinic dry static stability, M_{s1}, these are computed consistently from the vertical profiles. Allowing M_{s1} to vary with temperature, as in (3), renders the model unstable. Based on test runs to assess model stability, M_{s1} is set to a constant value of 3.27 K, or approximately 1 K higher than the reference value M_{sr1}.

2.3. Clouds, Radiation, and Surface Fluxes

[11] Cloud prediction is performed as in QTCM1, by assuming four cloud types (deep convective, cirrostratus, cirrocumulus, and stratus) with prescribed vertical structure. Shortwave and longwave radiative transfer coefficients are precomputed using the scheme of *Chou and Neelin* [1996] using the FT and ABL temperature and moisture basis functions in Figure 1. QTCM2 uses the SLAND1 land surface model as described in *Zeng et al.* [2000]. While QTCM1 estimates surface winds through a pseudo boundary layer, QTCM2 uses the boundary layer winds directly to estimate drag coefficients for surface fluxes.

2.4. Deep and Shallow Convection

[12] The deep convection scheme is identical to SN06, except a nonlinear scheme (as in QTCM1) is used to calculate the convective moisture profile using the saturation moisture dependence on temperature. A shallow convection parameterization is invoked when a quantity approximating convective available potential energy (CAPE) is negative. Shallow convection uses the relaxation scheme described in *Neggers et al.* [2007], with ABL convective heating, Qc_b, and drying, Qq_b, given by:
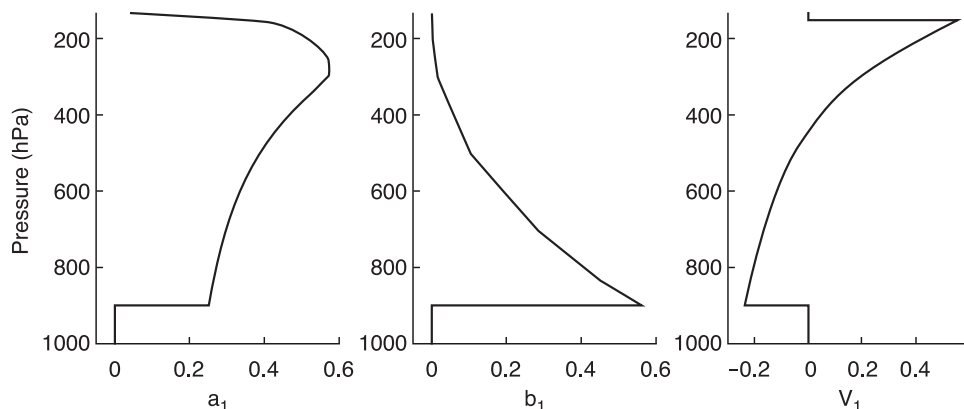
Figure 1. Vertical structure functions a1(p), b1(p), and V1(p) used in QTCM2.

Table 1. Baseline QTCM2 Parameter Values

Parameter	Value	Definition
p_s, p_e, p_t	1000, 900, 150 mb	Pressures at the surface, ABL top, and model top (tropopause)
$<a_1>^F, a_{1e}$	0.3958, 0.2531	Vertical integral and ABL top value of FT temperature basis function
$<b_1>^F, b_{1e}$	0.1789, 0.5634	Vertical integral and ABL top value of FT moisture basis function
$<a_1^+>^F$	0.2378	Logarithmic vertical integral of FT moisture basis function
$<a_b^+>^F, a_b^{+e}$	0.0513, 0.1038	Logarithmic vertical integral of ABL moisture basis function and ABL top value
$<V_1^2>^F, <V_1^3>^F/<V_1^2>^F$	0.0457, 0.2024	Coefficients for momentum advection
V_{1e}	-0.2378	Value of baroclinic mode velocity at the ABL top
$<a_1 V_1>^F, <b_1 V_1>^F$	0.0197	Coefficients in Ms1, Mq1
$T_{rb}, T_{re}, <T_r>^F$	302, 296.6, 263.57 K	Reference ABL, ABL top, and FT temperatures
$q_{rb}, q_{re}, <q_r>^F$	51.26, 38.84, 12.33 K	Reference ABL, ABL top, and FT moistures
M_{sr1}, M_{sr0}	3.27, 16.60 K	Reference dry static stabilities
M_{sp1}, M_{sp0}	0, 0.2107	Dry static stability changes per T1 change
M_{qr1}, M_{qr0}	1.99, 26.50 K	Reference moisture stratifications
M_{qp1}, M_{qp0}	0.0289, 0.3844	Moisture stratification changes per q1 change

$$Qc_b = \begin{cases} \dfrac{T_{1c}^{sh} - s_b}{\tau_{sh}} \\ \dfrac{q_{1c}^{sh} - q_b}{\tau_{sh}} \end{cases} \quad (4)$$

By definition, the net shallow convective heating and drying integrated over the entire depth of the troposphere have zero integral. Thus, in the FT, shallow convective warming and drying, Qc_f and Qq_f, are given by $(Qc_f, Qq_f) = -\dfrac{\Delta p_b}{\Delta p_f}(Qc_b, Qq_b)$. Here, the shallow convective reference temperature and moisture values T_{1c}^{sh} and q_{1c}^{sh} are given by the values of dry static energy and moisture just above the boundary layer:

$$\begin{aligned} T_{1c}^{sh} &= \begin{cases} s_{re} + a_{1e} T_1 \\ q_{re} + b_{1e} q_1 \end{cases} \end{aligned} \quad (5)$$

where s_{re} and q_{re} are reference values of dry static energy and specific humidity just above the ABL. As *Neggers et al.* [2007] note, the shallow convective adjustment timescale τ_{sh} can be related to the mixed layer depth z_b and the shallow cumulus mass flux m_b^{sh}, i.e., $\tau_{sh} \sim \dfrac{z_b}{m_b^{sh}}$, which is of order 10^5 s. Following *Neggers et al.* [2006], we implement a variable τ_{sh} by estimating the gridpoint convective velocity scale $w*$, which is related to the surface buoyancy flux and can be expressed in terms of surface sensible and latent heating as described in *Cuijpers and Bechtold* [1995].

2.5. Numerics

[13] We consider model simulations performed at both a fine resolution ($1.40625° \times 1°$) and the coarse ($5.625° \times 3.75°$ resolution) used as the default in QTCM1, with the model domain spanning 78.75°S–78.75°N. Fourier filtering is applied to prognostic variables to damp small-scale features for latitudes poleward of 45°. Note that while the latitudinal extent of the model and Fourier filtering domain can be adjusted, because we do not see strong indications of improvements in mid-latitude variability relative to QTCM1, we keep this aspect of the model the same to focus on the changes in the tropical variability associated with the additional vertical degree of freedom. The prognostic equations are finite differenced on an Arakawa-C grid. Time tendencies of each prognostic variable are stored as arrays, and updates are performed simultaneously for all prognostic variables using a simple first order scheme, using a 10 minute timestep. Diffusion coefficients are set to values 60% higher than assumed in QTCM1 for added stability. On a Sun Fire workstation, one year of simulation at the low resolution can be executed in under 2 minutes wall-clock time.

[14] Several switches are embedded in the code to facilitate implementation of different configurations of the model (see Section 4). For example, QTCM2 can be run in a "pseudo-QTCM1" configuration by slaving the FT and ABL thermodynamic and momentum equations; it is possible to run with slaved thermodynamics, slaved momentum, or both. Additional switches allow QTCM2 to be run with a QTCM1-like deep convection scheme and the original parameter set.

3. Baseline QTCM2 Climatologies for DJF

[15] Here we present a brief overview of the baseline climatologies of temperature, moisture, winds, and precipitation as simulated by QTCM2, focusing for simplicity on December-January-February (DJF). In what follows, we consider both the high- and low-resolution QTCM2 simulations. For temperature, moisture, and winds, we primarily focus on the ABL, as this represents, roughly-speaking, the added degree of freedom relative to QTCM1. Further discussion of precipitation appears in Sections 4 and 5. For comparison, we show comparable NCEP Reanalysis 2 [*Kanamitsu et al.*, 2002] temperature, moisture, and wind fields and Climate Prediction Center Merged Analysis of Precipitation (CMAP) [*Xie and Arkin*, 1997] precipitation.

[16] Relative to the NCEP Reanalysis 2 m DJF surface air temperatures (Figure 2a), QTCM2 surface air temperatures over the tropical oceans are generally low in the low resolution simulation (Figure 2c) especially in the eastern Pacific, while in the high resolution simulation (Figure 2b), the surface air temperature is too zonal in the southern Hemisphere. QTCM2-simulated DJF temperatures averaged over the depth of the troposphere (not shown) are more zonally-uniform than the surface air temperatures, as expected, although the band of warmest tropospheric mean temperatures in the deep tropics is somewhat too narrow. A cool bias in vertically-averaged temperature was noted in the axisymmetric simulations of *Bellon and Sobel* [2010] and is also evident in QTCM1 (not shown).

[17] Comparing reanalysis to simulated moisture (Figure 3), DJF near-surface specific humidity in QTCM2 at either resolution is pervasively low over much of the tropical ocean. This also holds for some
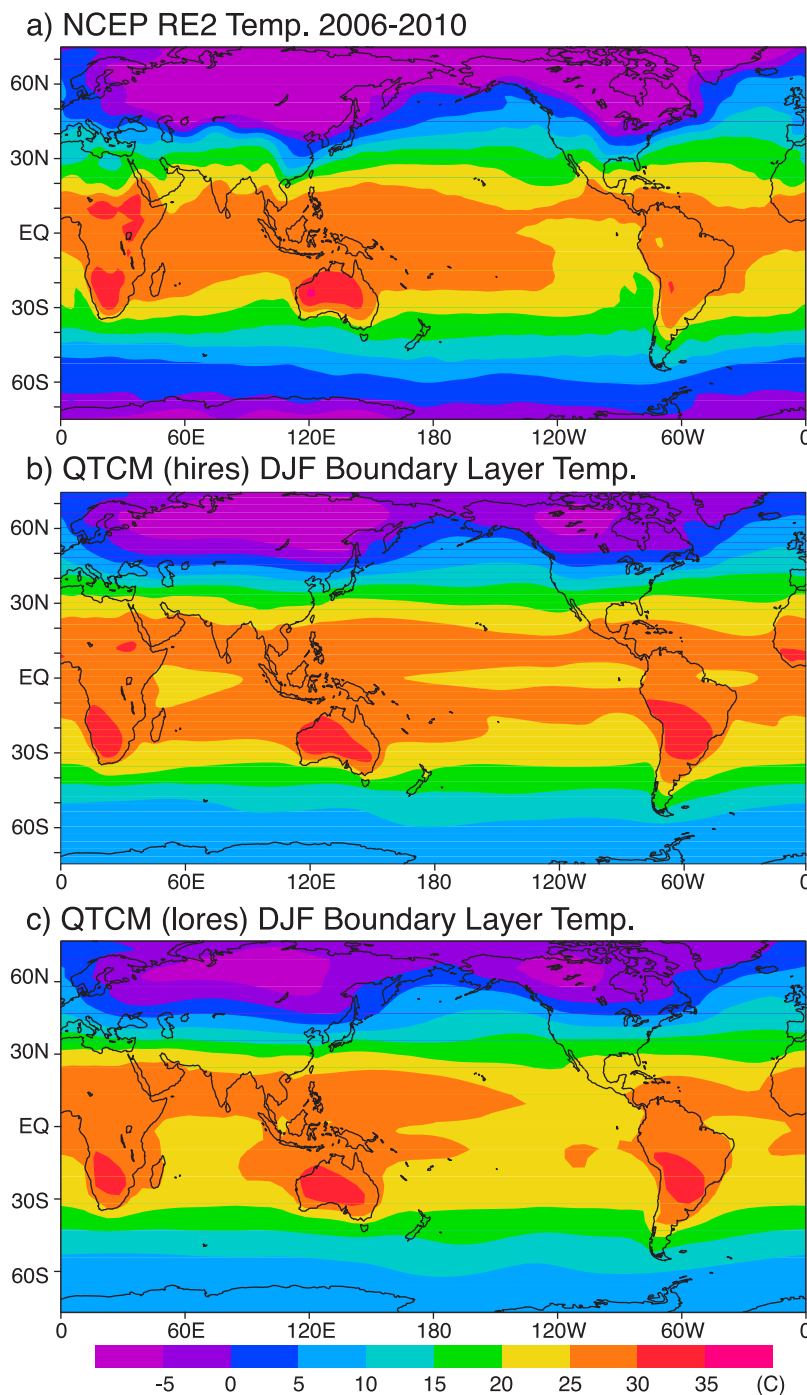
Figure 2. Comparison of DJF 2 m temperatures from (a) the NCEP Reanalysis 2 and QTCM2 at (b) high resolution and (c) low resolution. Units are in °C.
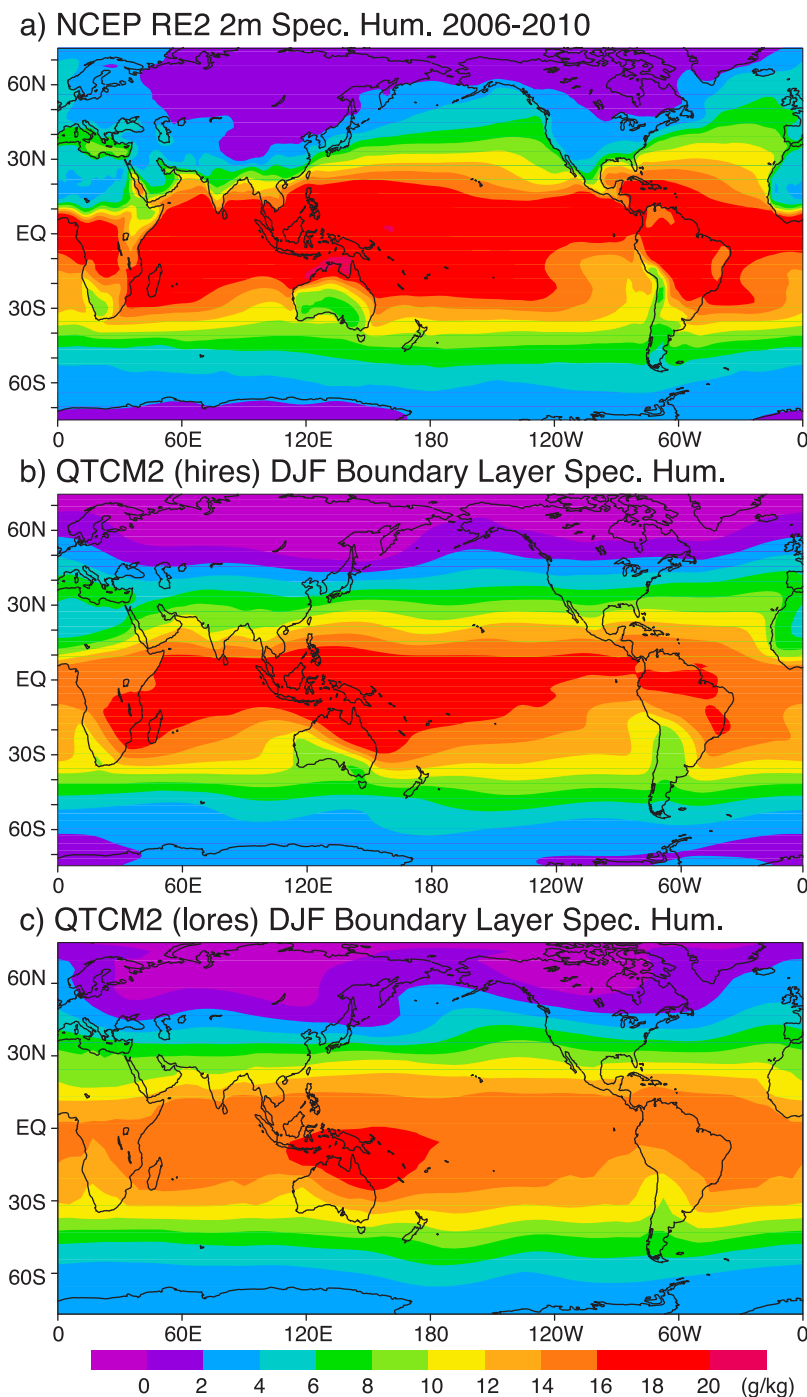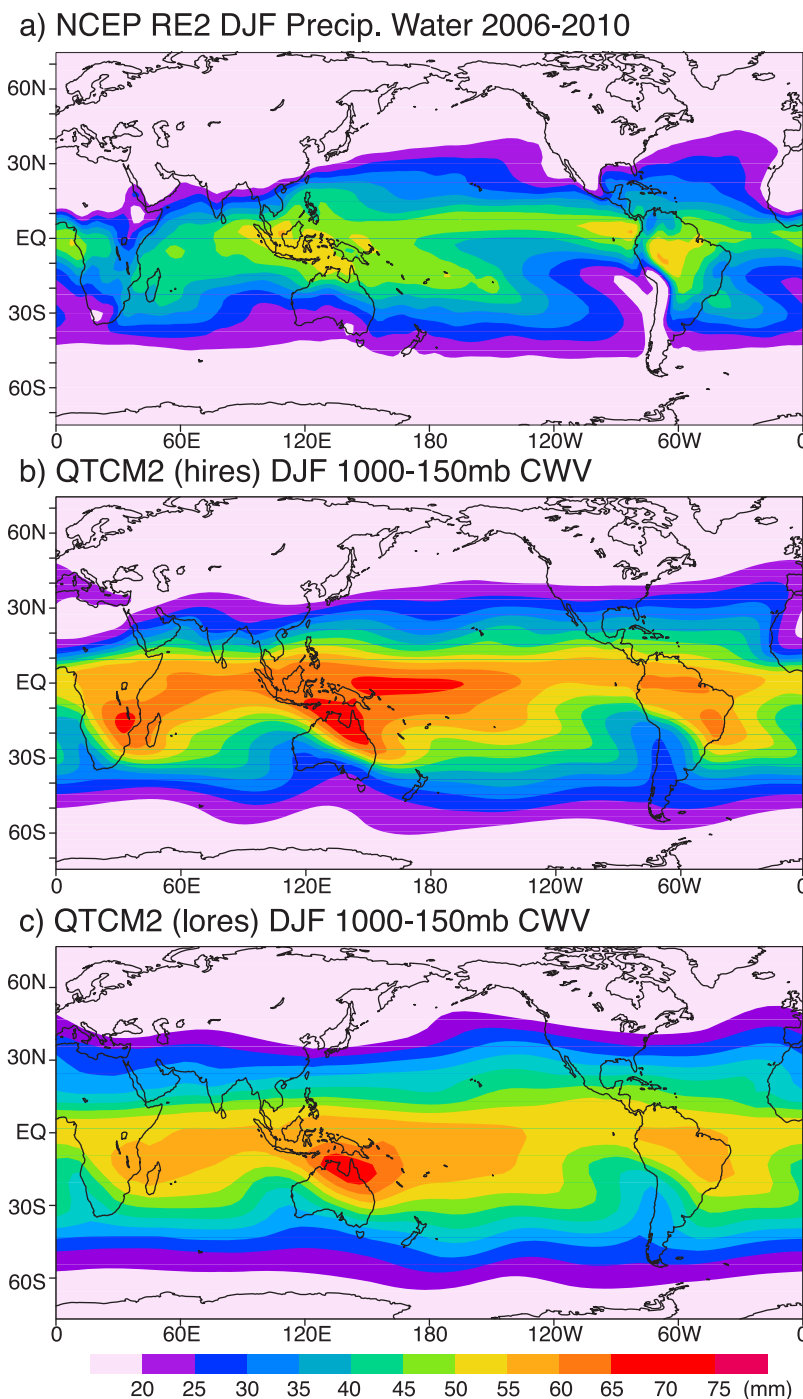
Figure 3. Comparison of DJF 2 m specific humidity from (a) the NCEP Reanalysis 2 and QTCM2 at (b) high resolution and (c) low resolution. Units are in g kg^{-1}.

land regions, although subtropical deserts in both hemispheres are too moist. Despite the tendency for too dry conditions over tropical oceans, the gross spatial distribution of near surface moisture in QTCM2 compares well to NCEP, e.g., the maximum DJF ABL moisture occurs just to the north of Australia. Also, we note the impact of increased spatial resolution, which somewhat mitigates the low bias over the ocean and high bias over the land. High values of reanalysis column water vapor (CWV) (Figure 4a) prevail in the low-latitudes of the

SH, with peak values exceeding 60 mm to the north of Australia and smaller maxima off the west coast of Africa and over South America. Overall, CWV as simulated by the baseline QTCM2 is high-biased near regions of intense tropical deep convection, especially at high resolution, although CWV can be tuned through the convection scheme or other parameters such as the moisture stratification.

[18] The DJF boundary layer winds (Figure 5, vectors) as simulated by QTCM2 are broadly consistent

a) NCEP RE2 DJF Precip. Water 2006-2010

b) QTCM2 (hires) DJF 1000-150mb CWV

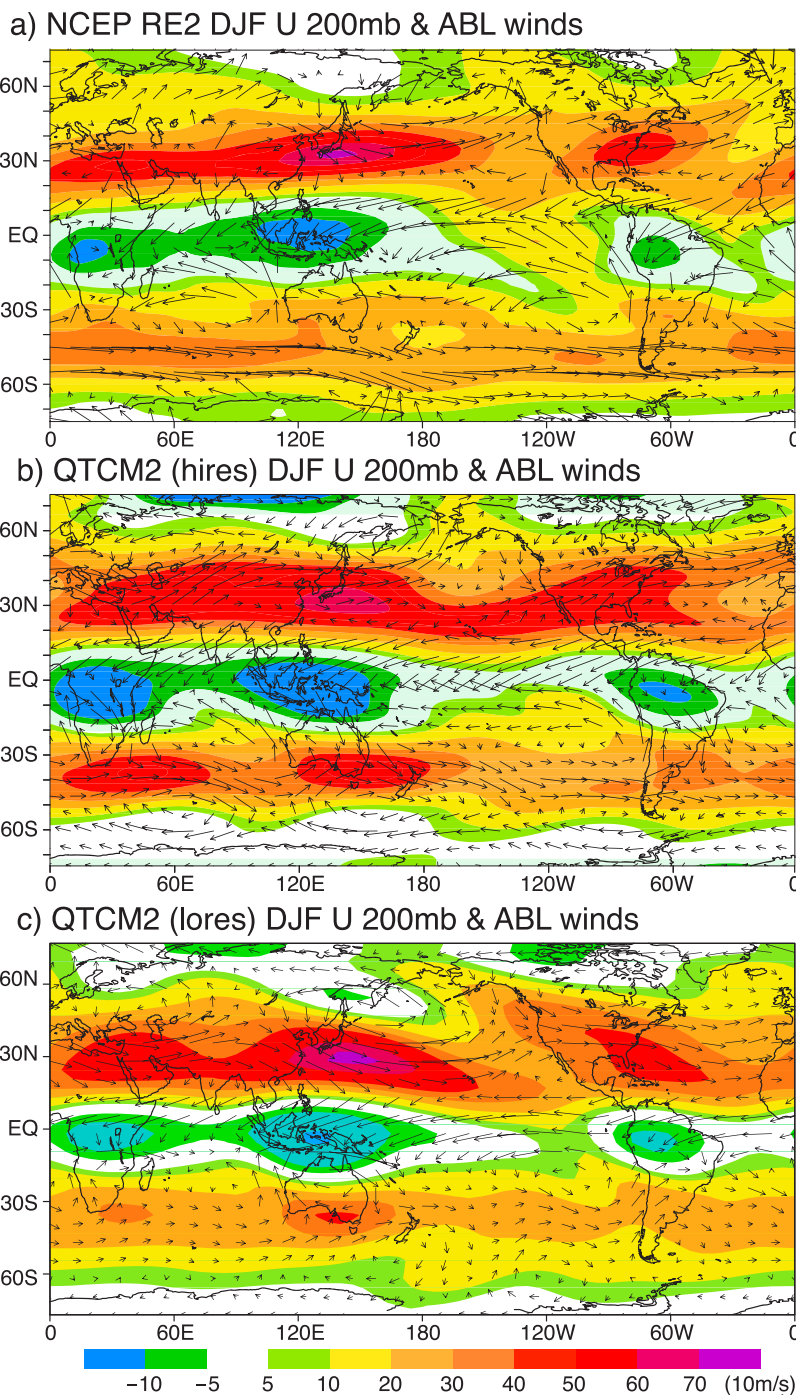c) QTCM2 (lores) DJF 1000-150mb CWV

Figure 4. Comparison of DJF CWV from (a) the NCEP Reanalysis 2 and QTCM2 at (b) high resolution and (c) low resolution. Units are in mm.

with the leading features in the reanalysis, although the winds for the low resolution simulation (Figure 5c) are more zonal in the eastern Pacific and Atlantic. Also, only the high resolution simulation captures the "roaring 40 s" westerlies in the SH. At 200 mb, both the high and low resolution QTCM2 configurations simulate easterlies over the deep Tropics (Figure 5b, filled contours), with localized centers near tropical continents. In the NH midlatitudes, westerly wind maxima are found over the mid-East and in jet regions east of Japan and along the eastern coastline of North America. However, the jet axes tilt unrealistically toward the southeast. The upper tropospheric meridional winds (not shown) tend to be somewhat larger than observed, and for both the zonal and meridional components, the values are larger than simulated by QTCM1 (not shown).

[19] For precipitation (Figure 6), QTCM2 manifests the principal DJF tropical spatial features as seen in the

a) NCEP RE2 DJF U 200mb & ABL winds

b) QTCM2 (hires) DJF U 200mb & ABL winds

c) QTCM2 (lores) DJF U 200mb & ABL winds

Figure 5. Comparison of DJF winds from (a) the NCEP Reanalysis 2 and QTCM2 at (b) high resolution and (c) low resolution. Shown are boundary layer winds (vectors; values relative to the reference arrow) and 200 mb zonal wind (shading; units of m s^{-1}). For visual clarity in Figures 5b and 5c, vectors are only plotted for every 10° in longitude and 7° degrees in latitude.

CMAP data in the broadest sense at both resolutions, but there are significant differences, beyond simply the sharpness of the gradients, between the low-resolution and high-resolution models. For tropical land regions, precipitation maxima are present over Africa, the maritime continent, and South America. Structurally, these maxima tend to comprise single centers in the low resolution version (Figure 6c) but multiple centers at higher resolution (Figure 6b). ITCZs are evident over the Atlantic, Indian, and eastern Pacific Oceans, although these are generally weak compared to the observations. The East Pacific ITCZ is also located somewhat too far south of its observed DJF position. At least for DJF, the ITCZ structure appears to be

a) CMAP DJF Precip.

b) QTCM2 (hires) DJF Precip.

c) QTCM2 (lores) DJF Precip.
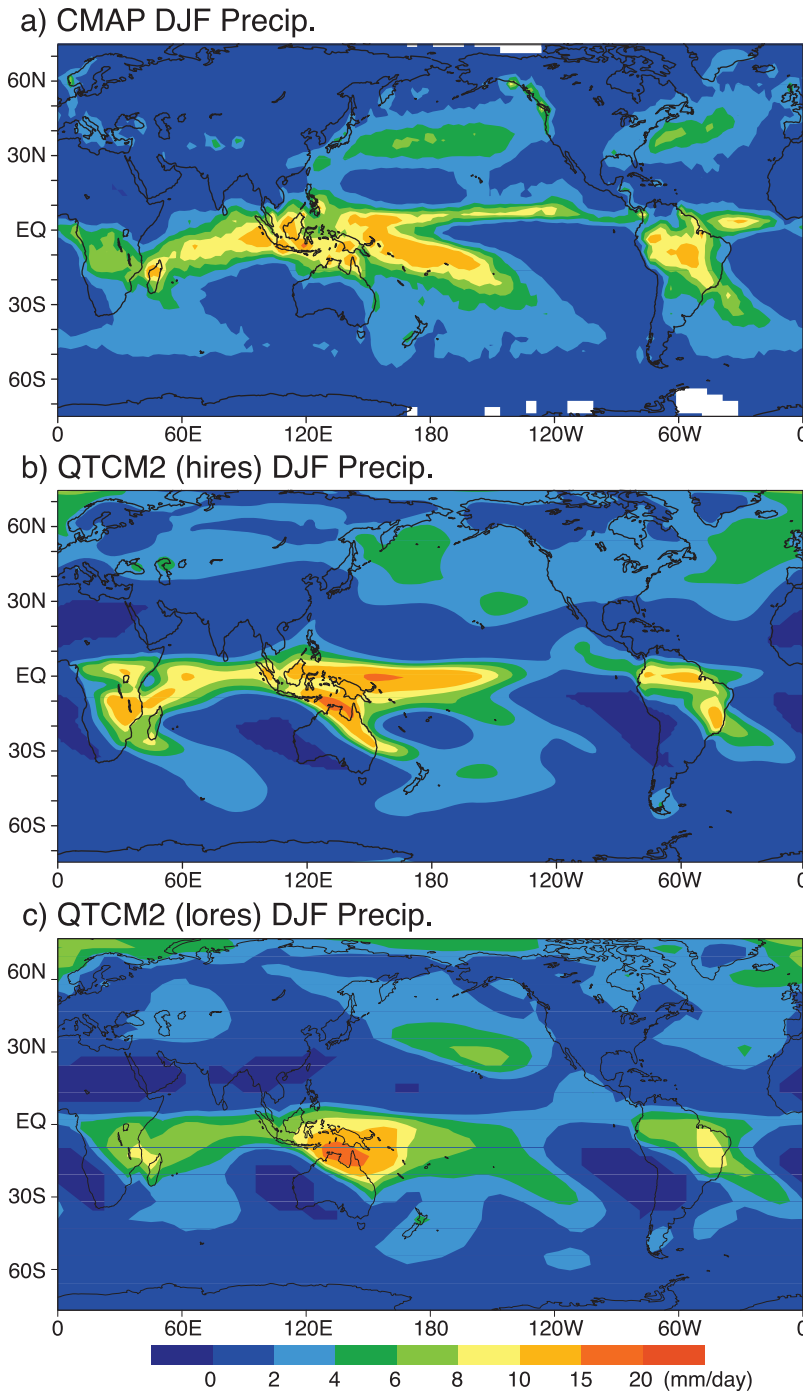
Figure 6. Comparison of DJF precipitation from (a) CMAP and QTCM2 at (b) high resolution and (c) low resolution. Units are in mm day^{-1}.

better captured than in QTCM1, which is consistent with the arguments presented in SN06, although the improvements may not be as pronounced as in the axisymmetric model. Perhaps unsurprisingly, the simulation of narrow features such as ITCZs is rather sensitive to model resolution. The tilted, tropical-subtropical South Pacific and South Atlantic Convergence Zones (SPCZ and SACZ) are present, but penetrate too far into the (non-deep convecting) dry descent regions observed over the southeastern tropical Pacific and

Atlantic Oceans. In the tropical West Pacific, there is also a large precipitation dipole bias between the SPCZ and the eastern coast of Australia.

4. Isolating How the Implementation of QTCM2 Impacts Precipitation

[20]　In this section, we are interested in further assessing how the implementation of the new physics in QTCM2 contributes to the model's precipitation behavior. For the

results discussed hereafter we consider the coarse resolution simulations unless otherwise noted.

4.1. Overview of QTCM1 Precipitation Behavior

[21] Since we are interested in how inclusion of the ABL modes impacts the simulated precipitation in QTCM2, we briefly highlight a few aspects of the precipitation field as simulated by its predecessor model, QTCM1. (For reference, the QTCM1 DJF precipitation field at the coarse resolution is depicted in Figure 7.) In general, QTCM2 produces stronger oceanic ITCZs than does QTCM1; furthermore, QTCM2 tends to produce less rainfall over tropical land than does QTCM1. Thus, while QTCM1 greatly underestimates the ratio of oceanic to land region precipitation in the tropics relative to the observations, this ratio is improved (albeit still too low) in QTCM2.

4.2. Precipitation Sensitivity to Added Physics in QTCM2

[22] As noted in Section 2, implementation of QTCM2 differs from QTCM1 in three principal ways: (i) *model physics associated with the boundary layer degree of freedom*; (ii) *model parameterization schemes*; and (iii) *model parameters*. In this section, we consider how these differences impact the simulation, especially precipitation. To address the model sensitivity to the addition of a decoupled ABL, we consider a model configuration in which temperature and moisture are obtained from vertically-averaged tendencies of ABL and FT temperature and moisture and ABL values of dry static energy and moisture prescribed to FT T_1 and q_1 extrapolated to their mean values in the ABL:

$$\frac{dT_1'}{dt} = \frac{\Delta p_f (dT_1/dt) + \Delta p_b (ds_b/dt)}{a_1^f \Delta p_f + a_1^b \Delta p_b}; \quad s_b' = a_1^b T_1$$

$$\frac{dq_1'}{dt} = \frac{\Delta p_f (dq_1/dt) + \Delta p_b (dq_b/dt)}{b_1^f \Delta p_f + b_1^b \Delta p_b}; \quad q_b' = b_1^b q_1 \tag{6}$$

Momentum is slaved by setting ABL zonal and meridional winds to the total (barotropic+baroclinic) velocity at the base of the FT. Additionally, the tendencies of FT baroclinic wind momentum are adjusted to account for the affect of ABL convergence on forcing the FT baroclinic mode, while the barotropic mode is constrained to be nondivergent as in QTCM1. Thus:

$$\frac{d\mathbf{v}_1'}{dt} = \frac{\Delta p_f V_1^{2F}(d\mathbf{v}_1/dt) + \Delta p_b V_{1pe}(d/dt)(\mathbf{v}_b - \mathbf{v}_0)}{\Delta p_f V_1^{2F} + \Delta p_b V_{1pe}^2};$$

$$\mathbf{v}_b' = \mathbf{v}_0 + V_{1pe}\mathbf{v}_1 \tag{7}$$

Relative to the baseline QTCM2 simulation, DJF precipitation is generally weakened when the ABL and FT are slaved (Figure 8a, light gray shading depicts where precipitation in the coupled modes configuration is reduced relative to the baseline). In fact, for the tropical regions which are more weakly convecting in the model, precipitation is reduced by 50% or more when the ABL and FT are slaved. Some of these regions which are sensitive to the presence or absence of ABL dynamics are also weakly convecting in observations, while others are more strongly convecting in observations but biased dry in the model, particularly in the absence of ABL dynamics. The East Pacific ITCZ in particular is largely suppressed with ABL-FT slaving, consistent with the arguments of SN06 [see also *Sobel*, 2007]. Such behavior broadly mirrors the precipitation differences between the baseline QTCM2 and QTCM1 (Figures 6c and 7, respectively).

[23] By separately slaving ABL and FT thermodynamic and dynamic modes, we can infer the contributions of each of the added thermodynamic and dynamic degrees of freedom to the differences in QTCM2. Like the precipitation differences in Figure 8a, those associated with coupled thermodynamics (Figure 8c) are largely negative throughout the Tropics, except along
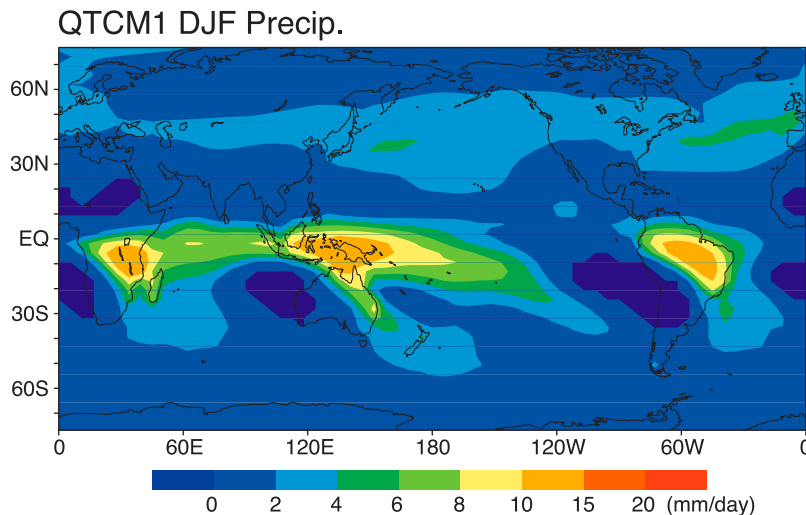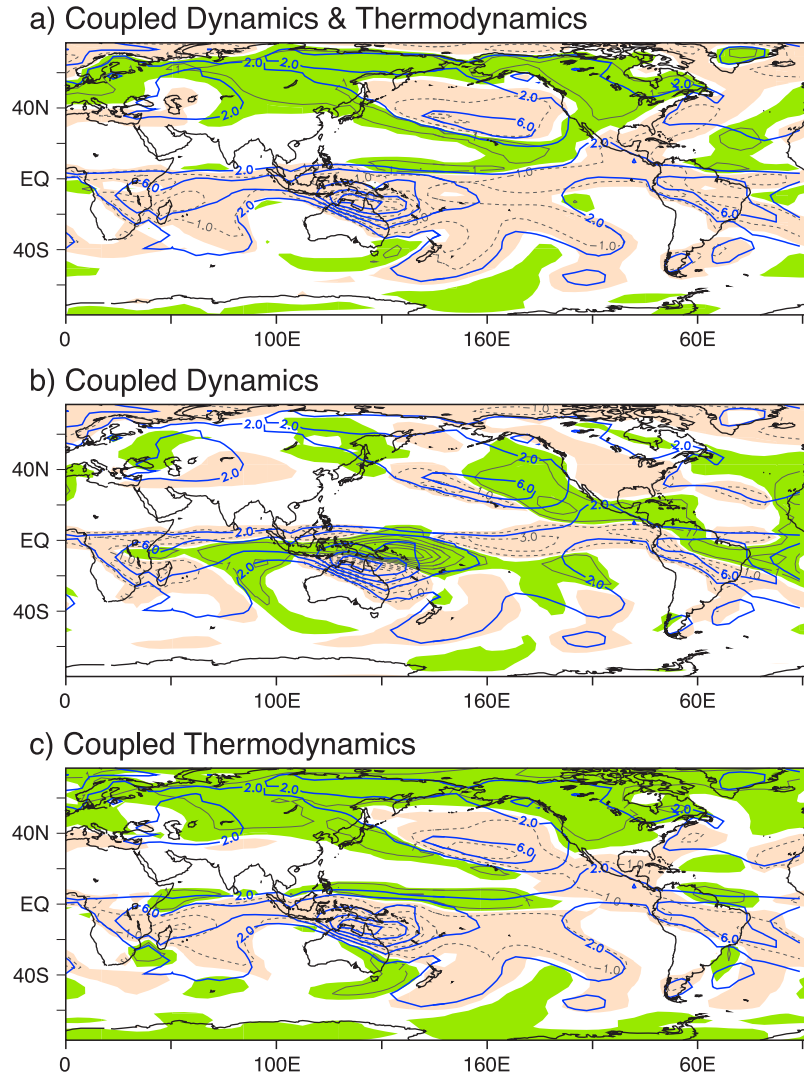

Figure 7. As in Figure 6, but for QTCM1.

a) Coupled Dynamics & Thermodynamics

b) Coupled Dynamics

c) Coupled Thermodynamics

Figure 8. QTCM2 sensitivity to independent ABL and FT thermodynamics and dynamics. (a) Impact of slaving ABL and FT dynamics and thermodynamics on January precipitation. Gray contours show precipitation differences of the coupled minus baseline simulations, with a contour interval of 1 mm day^{-1} and the zero contour omitted. Tan and light green shading further highlight gridpoints for which the precipitation differences are, respectively, negative and positive with a magnitude of at least 0.25 mm day^{-1}. For reference, January precipitation from the baseline QTCM2 is shown (blue contours). (b) As in Figure 8a, but slaving dynamics only. (c) As in Figure 8a, but slaving thermodynamics only.

certain convective margins such as the northern edge of the western Pacific warm pool/East Pacific ITCZ. The effect of coupling dynamics, by contrast, produces both negative and positive differences relative to the baseline case (Figure 8b). Indeed, when ABL and FT momentum modes are slaved, DJF precipitation is enhanced over much of the western Pacific warm pool but weakened in the eastern Pacific ITCZ. The presence of nonlinearities such as those in the model deep convection scheme gives rise to some modest regional scale differences between the differences in Figure 8a and the sum of differences in Figures 8b and 8c.

[24]   One of the principal objectives in constructing a two-level QTCM in SN06 was to achieve better simulation of features such as ITCZs, for which ABL convergence and the Lindzen-Nigam mechanism are expected to play a role. The results here confirm that the added physics in the full QTCM2 do have a demonstrable impact.

4.3.   Sensitivity to the Revised Deep Convection Scheme

[25]   We also consider the impact of the convection scheme in QTCM2 by implementing a convection scheme closer to the existing scheme in QTCM. In this implementation, CAPE (or a CAPE-related quantity) is computed over the entire depth of the troposphere using troposphere-averaged temperature $\langle T \rangle$ and moisture $\langle q \rangle$, namely:

$$\langle T\rangle = \begin{cases} \dfrac{\Delta p_b s_b + \Delta p_f a_1^f T_1}{\Delta p_b + \Delta p_f} + \langle T_{ref}\rangle \\[3mm] \dfrac{\Delta p_b q_b + \Delta p_f b_1^f q_1}{\Delta p_b + \Delta p_f} + \langle q_{ref}\rangle \end{cases} \quad (8)$$

The tropospheric-averaged deep convective heating rate, Qc_t, is equivalent to CAPE divided by the timescale for convective adjustment τ_c, i.e.,

$$Qc_t = \frac{CAPE}{\tau_c} = \frac{\langle T_c\rangle - \langle T\rangle}{\tau_c}; \quad CAPE > 0 \quad (9)$$

where $\langle T_c\rangle$ is a vertically-averaged convective reference temperature profile. Assuming total enthalpy is conserved during deep convection, the sum of convective heating and convective drying, Qq_t, is zero. ABL convective heating and drying are computed as in the standard configuration of QTCM2, i.e., assuming a boundary layer moist static energy perturbation, while FT convective heating and drying are obtained as residuals based on the total heating and drying and the ABL values.

[26] Differencing the QTCM1 convection configuration from the baseline QTCM2 shows increasing precipitation along many of tropical convective margins (Figure 9). At the same time, within the cores of convecting regions, precipitation rates decrease with the implementation of QTCM1 deep convection. The former likely results from the condition of positive CAPE for the triggering of deep convection, which becomes a weaker constraint with the alternative computation of CAPE, while the latter likely results from compensating mechanisms between margins and cores of the convecting regions. We note that the stronger precipitation in the Pacific and Atlantic ITCZs with the QTCM1 scheme implies that enhancement of the ITCZs due to the additional vertical degree of freedom in QTCM2 has been partially compensated by the change in convective closure described in SN06, and this may be of interest for examination in future work.

4.4. Sensitivity to Revised Parameters

[27] Reverting to the vertical structure functions $a_1(p)$, $b_1(p)$, and $V_1(p)$ used in QTCM1 (Figure 10) causes

precipitation within regions of strongest tropical deep convection to intensify and become more localized: within the cores of these regions, precipitation rates of ~ 30 mm day^{-1} are simulated. On the other hand, precipitation is strongly suppressed everywhere outside of the strongest convecting regions. The results presented here suggest that the revised or altered model parameters and parameterizations play a significant, nontrivial role in accounting for differences between QTCM2 and QTCM1; in fact, the differences attributable to parameter or parameterization changes are comparable to, and may even locally exceed, those associated with the additional physics.

5. Sensitivity Analyses for Deep and Shallow Convection and FT Moisture

[28] As a demonstration of the utility of the QTCM2 framework, we consider here some aspects of model convection schemes that are poorly constrained. Because simulated convective processes in climate models are very sensitive to parameterization [*Jackson et al.*, 2008], it is clearly of interest to explore how tropospheric moisture and precipitation are related in convective parameterizations.

5.1. Sensitivity to Deep Convective Adjustment Timescale

[29] One of the parameters poorly constrained in QTCM2 and many other models with similar convection schemes is the convective adjustment timescale τ_c, i.e., the time necessary to consume CAPE and relax the convective instability [*Jackson et al.*, 2008]. While the deep convective adjustment timescale was set to 2 hours in *Betts and Miller* [1986], *Bretherton et al.* [2004] have shown this parameter to be strongly scale dependent, with values that may be up to an order of magnitude larger. Note that the precipitation rate in QTCM2 is equivalent to the total deep convective heating rate averaged over the depth of the troposphere, since there is no stratiform precipitation.

[30] A comparison of QTCM2-simulated precipitation for January for τ_c of 6 hours, the default value assumed in QTCM2, and 2 hours, as assumed in QTCM1, is presented in Figure 11a. The most prominent difference here is the disappearance of the East Pacific ITCZ as τ_c is decreased. To see this, we note that
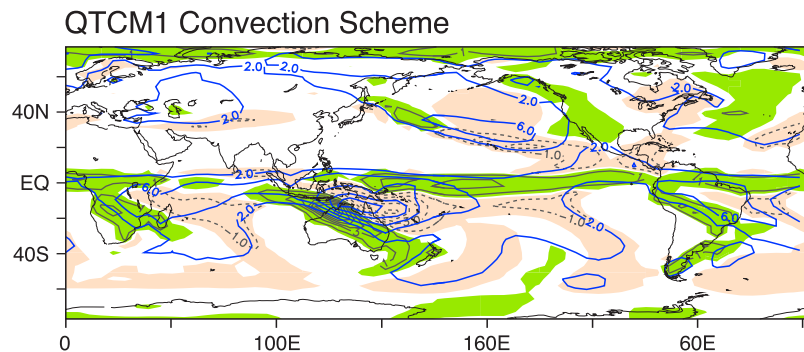
Figure 9. As in Figure 8, but for a configuration using QTCM1 deep convection scheme minus the baseline.

QTCM1 Basis Functions/Parameters
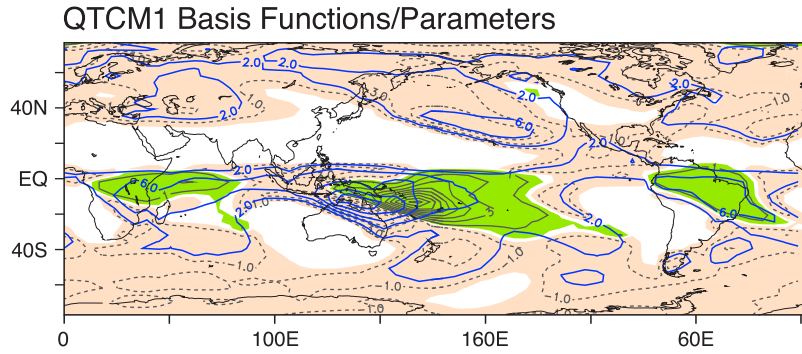
Figure 10. As in Figure 8, but for a configuration using the QTCM1 vertical structure functions minus the baseline.

the differences along the east Pacific ITCZ as depicted in Figure 11a are comparable to the baseline precipitation rates in Figure 6c. On the other hand, peak precipitation rates in the core regions of tropical deep convection, such as near the maritime continent, are typically enhanced as τ_c becomes smaller.

[31] To provide further insight into the precipitation sensitivity to the rate of deep convective adjustment, Figure 11b illustrates ABL and FT moisture differences for the two cases (2 hours minus 6 hours). Within the most strongly convecting tropical regions, ABL moisture (shading; in g kg^{-1}) is typically reduced for small τ_c. On the other hand, moister ABL conditions tend to prevail along the margins of strong tropical deep convection for τ_c = 2 hours. Within the FT, moisture loading is generally lower throughout the entire tropical troposphere for lower τ_c, as is total column water vapor.

[32] Our interpretation of these results is as follows. In strongly convecting regions or at times when strong tropical deep convection is present, lowering τ_c renders the local FT moisture sink more efficient, so that when the conditions for deep convection are met, moisture is rapidly removed. The faster removal of FT moisture within strongly convecting regions means that, away from these regions, less moisture will generally be available, as FT moisture transport into adjacent regions will be reduced. In marginally-convecting regions, the FT drying is especially crucial—even as the ABL itself is more humid at lower τ_c, the triggering of deep convection is inhibited by the drier FT. With faster deep convective adjustment, FT convective heating in strongly convecting cores is also enhanced; the additional heating in regions of deep convection sets up anomalous Gill-like responses that warm and dry the entire tropical FT.

a) Precipitation

b) ABL and FT Moisture
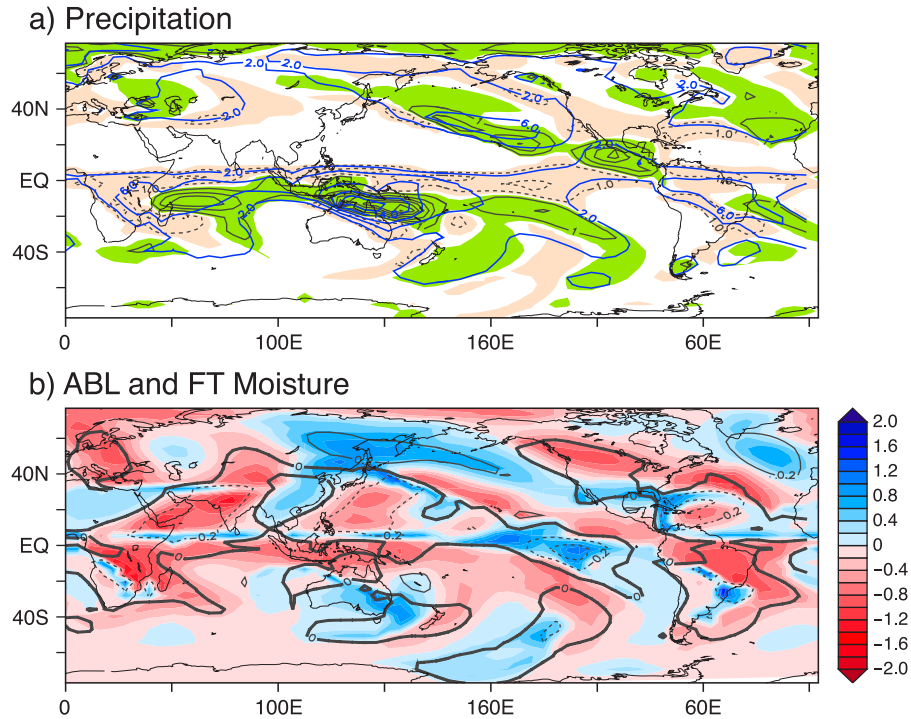
Figure 11. (a) As in Figure 8, but for a configuration with a deep convective adjustment timescale of 2 hours minus the baseline. (b) ABL and FT moisture differences (shading and contours, respectively), in units of g kg^{-1}.

## 5.2. Sensitivity to Shallow Convective Adjustment Timescale

[33] Here we consider sensitivity of QTCM2 to τ_{sh} by comparing the baseline simulation to one for which the shallow convective times are increased by a factor of 10 ("slow shallow adjustment"). Figure 12a illustrates the January precipitation differences between the slow shallow and baseline simulations. It can be seen that damping shallow convective adjustment is associated with decreasing marginal precipitation rates and (slightly) increasing precipitation away from the margins, although not necessarily where deep convection and precipitation tend to be strongest in the baseline simulation. With slow shallow convective adjustment, the ABL is strongly moistened just to the north of the equator outside of the strong convecting region (Figure 12b), with widespread reduction in free tropospheric moistening throughout the Tropics.

[34] The shallow convective sensitivity results described here are consistent with *Neggers et al.* [2007] (e.g., cf. Figure 4c of *Neggers et al.* [2007], which is for July rather than January). Of course, the version of QTCM used by *Neggers et al.* [2007] had two modes in moisture but retained the single mode in temperature and associated momentum modes from QTCM1. We note that altering shallow convective adjustment in each of moisture and temperature separately is found to have additive effects, with roughly half of total response coming from the moisture and temperature adjustments.
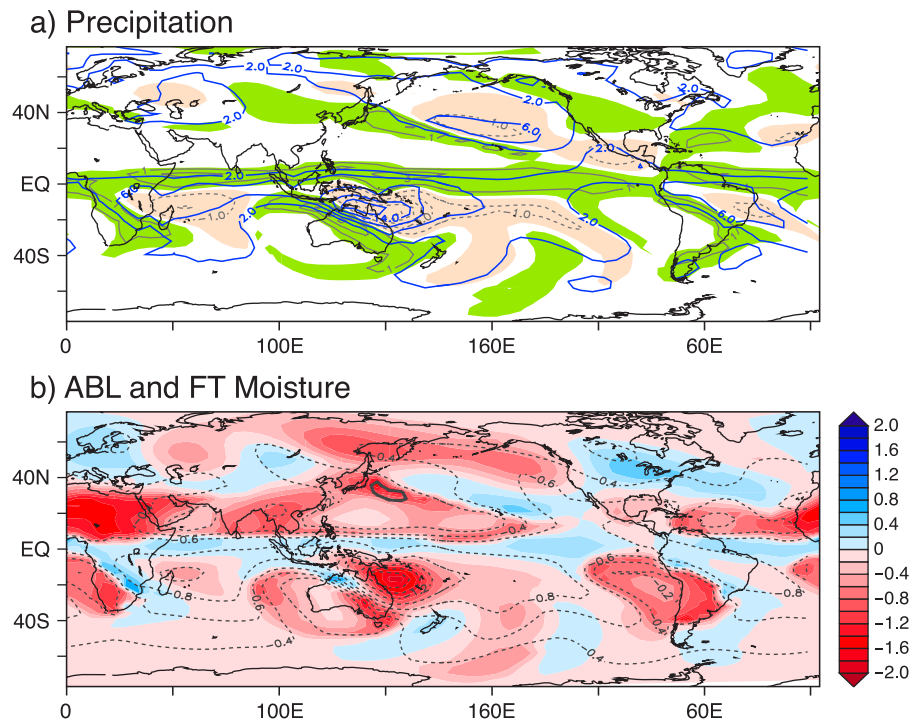
5.3. Decreasing Subsaturation

[35] A planned target for future work is to implement a mass flux scheme into QTCM2 by suitable projection of such a scheme onto QTCM2 basis functions. Of course, inclusion of a mass flux scheme in QTCM2 will require taking into account the effects of various processes, including entrainment, detrainment, subsidence, rain reevaporation, and at present, it is not obvious how this should be done. However, in anticipation of such an approach, we consider two simplifying approaches that might be viewed as approximating some features of an entraining plume model. The first approach is to adjust the subsaturation parameter, α, appearing in the computation of the FT convective reference profile. The Betts-Miller scheme uses this subsaturation parameter in its moisture reference profile (toward which moisture is adjusted) to loosely mimic the bulk impact of condensation, conversion to precipitating hydrometeors, precipitation, detrainment and reevaporation processes that would occur in a plume model without the need for detailed consideration of all processes involved.

[36] Figure 13 depicts the impact of uniformly reducing the default vertical subsaturation profile by 20%. Overall, lowering α tends to enhance precipitation along tropical convective margins or narrow ITCZs (e.g., the East Pacific ITCZ) while reducing precipitation within the core regions (Figure 13a). Moreover, the decrease in the subsaturation profile is associated with weak increases to ABL moisture where marginal precipitation is enhanced but decreases in ABL moisture elsewhere

a) Precipitation

b) ABL and FT Moisture
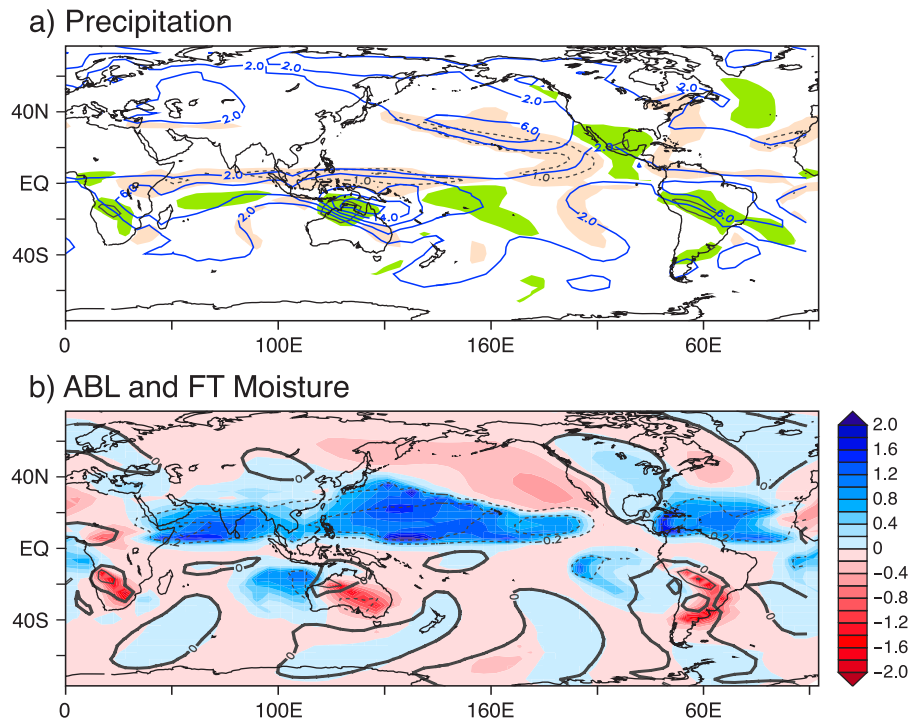
Figure 12. As in Figure 11, but for a configuration with shallow convective adjustment times multiplied by 10 minus the baseline.

a) Precipitation



b) ABL and FT Moisture

Figure 13. As in Figure 11, but for a configuration with FT subsaturation decreased by 20% minus the baseline.

and with pervasive drying of the FT. To understand these changes, we note that lowering α reduces the target for the convective adjustment, so that the troposphere ultimately adjusts toward a drier state. At the same time, the convective threshold condition, $q > q_c(T)$, is lowered, so convection can occur at lower ambient moisture; thus, precipitation in marginal regions can increase and/or expand. One subtlety here is that the lowering of $q_c(T)$ associated with lower subsaturation is somewhat offset by increased warming in the free troposphere, which drives up the saturation values and thus reduces convective instability. The overall pattern for lower subsaturation resembles the (inverse of) the rich-get-richer mechanism [*Neelin et al.*, 2003].

5.4.   Adding an Entrainment-Like Process

[37]   The second approach for approximating a more realistic entraining type model in QTCM2 involves adding an entrainment-like process to the convective closure, specifically one that mimics the effect of free tropospheric moisture on plume temperature structure. Indeed, the baseline convection scheme in QTCM2, like in QTCM1, assumes a parcel associated with a given ABL moist static energy perturbation would follow a moist adiabat through the FT, so that no effect of environmental mixing is assumed. To include one of the most important effects of entrainment, we modify the computation of the convective reference temperature in the deep convection scheme by including a term proportional to the FT moisture deficit relative to saturation. This simple form is suggested by recent results of *Sahany et al.* [2012] showing how entraining CAPE decreases as a function of FT relative humidity and the strength of entrainment.

[38]   Enabling the simple entrainment-like term leads to decreased precipitation along tropical convective margins (Figure 14a), which is consistent with expectations, since regions bounding the convection zones are likely to be farther from saturation, such that entrainment of relatively dry air there leads to an increase in the plume lapse rate in the free troposphere, which will tend to reduce the CAPE-like quantity $(T - T_c)$, with attendant reduction in convective precipitation. Core convecting regions are seen to experience increasing precipitation when the entrainment-like term is enabled. Such behavior likely represents the operation of processes involving elements of the rich-get-richer mechanism and the feedbacks discussed by *Neggers et al.* [2007]. The moisture required for convective instability is slightly increased for a given large-scale temperature due to the entrainment-like effect. Reduction in rainfall near the convective margins would yield a slight reduction in tropospheric temperature if this were not compensated by other adjustments. Constraints applying to a tropics-wide scale lead to slight adjustments in tropospheric temperature to keep to convective heating averaged over the entire Tropics from changing as strongly as occurs locally. This leaves the core of the convective regions at a slight advantage for convective instability relative to the convective margins. The moisture that fails to precipitate out in marginal regions ultimately winds up within the convecting core regions. Similar effects in the response to entrainment can be seen in full climate models (B. Oueslati and G. Bellon, Convective entrainment and large-scale organization of tropical precipitation: Sensitivity of the CNRM-CM5 hierarchy of models, submitted to *Journal of Climate*, 2012).

a) Precipitation

b) ABL and FT Moisture
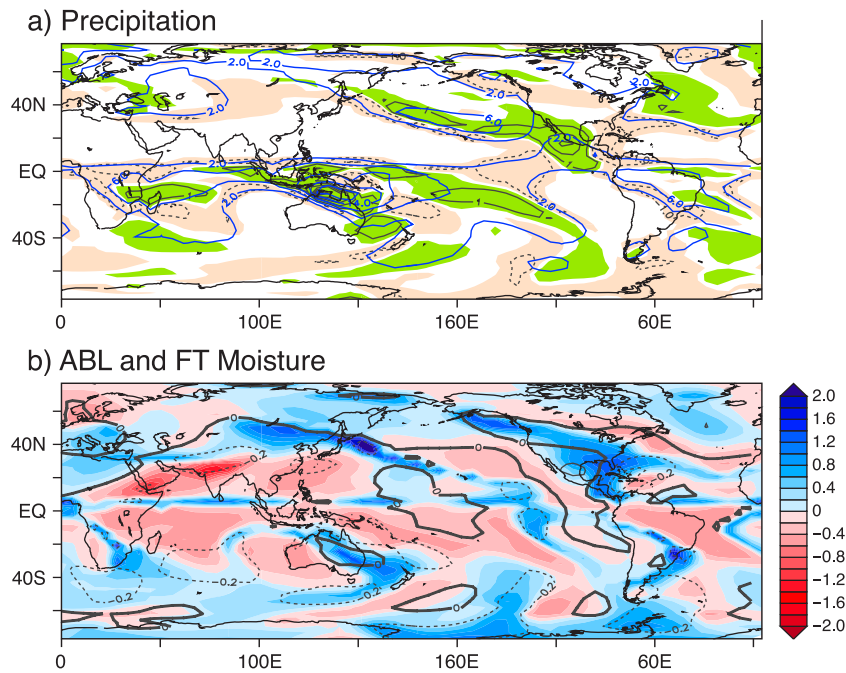
Figure 14.   As in Figure 11, but for a configuration with entrainment added minus the baseline.

6.   Summary and Conclusions

[39]   In this paper, we describe the implementation of the Quasi-equilibrium Tropical Circulation Model 2 (QTCM2), a two-level intermediate level complexity model. Following the approach of *Sobel and Neelin* [2006], a prognostic atmospheric boundary layer of fixed depth is added. Free-tropospheric basis functions are re-defined accordingly between the boundary layer top and nominal tropopause, but are otherwise similar to those used in QTCM1. Projecting the primitive equations on the ABL plus FT yields twice as many prognostic equations as in QTCM1 for thermodynamic quantities, and one new set of momentum equations for the ABL in addition to the baroclinic and barotropic free-tropospheric modes.

[40]   QTCM2 is shown to produce reasonable climatologies of temperature, moisture, winds, and precipitation. While some aspects of the simulated behavior in QTCM2 do improve relative to the predecessor model (QTCM1)—e.g., partitioning of land versus ocean precipitation—not all features are clearly improved. Despite this, we maintain that the model's utility lies in applications to problems for which the original model was not suited, such as addressing the influence of FT moisture on tropical deep convection.

[41]   As noted in SN06 and several studies with idealized versions of QTCM2 [*Bellon and Sobel*, 2008a, 2008b, 2010], the addition of ABL physics does produce some differences relative to the single mode predecessor, such as the strengthening of precipitation in Intertropical Convergence Zones (ITCZs). It should be pointed out, however, that changes to model parameters, stemming primarily from use of revised vertical structure functions, as well as model parameterizations are found to impact QTCM2-simulated precipitation as much as the added physics. In light of QTCM2's sensitivity to parameter changes, we suggest that the model may represent a useful testbed for parameter optimization techniques.

[42]   We also document some aspects of QTCM2's convective sensitivity to vertical moisture structure. Adjustments to the model convection scheme, such as alterations to the tropospheric subsaturation profile or inclusion of FT entrainment, demonstrate how basic physical processes impact QTCM2-simulated precipitation. From various convective sensitivity experiments conducted, we note several common features in the simulated precipitation response, namely: (i) increasing precipitation is associated with increasing column water vapor; (ii) strengthening of vertical moisture gradients, with either larger increases or smaller decreases in ABL moisture relative to the FT, is associated with decreasing precipitation; and (3) feedbacks between moist dynamics and convective processes may produce complex spatial behavior. The occurrence of trade-offs between precipitation sensitivity in the core convecting regions and their margins, and the mechanisms for these trade-offs, may provide prototypes for interpreting similar sensitivity evident in more complex models.

[43]   Finally, we note several targets for future model improvement, including implementation of a cumulus mass flux scheme; revised cloud prediction, especially the addition of an explicit stratocumulus parameterization; and the addition of large-scale precipitation. In the spirit of community-oriented model development, we welcome and encourage efforts to refine or add to QTCM2 physics and parameterizations.

Appendix A

[44] The horizontal velocity, $\mathbf{v}=(u, v)$; pressure vertical velocity ω; temperature T in energy units, i.e., temperature in Kelvin multiplied by c_p, the heat capacity of air at constant pressure; and specific humidity q in energy units, i.e., specific humidity in $kg\,kg^{-1}$ multiplied by the latent heat of vaporization L_v, satisfy the primitive equations in pressure coordinates:

$$\frac{d\mathbf{v}}{dt} + \omega\partial_p\mathbf{v} + f\hat{\mathbf{k}}\times\mathbf{v} = -\nabla\varphi + \mathbf{F}_v \qquad (A1)$$

$$\frac{dT}{dt} + \omega\partial_p s = Q_c + Q_R \qquad (A2)$$

$$\frac{dq}{dt} + \omega\partial_p q = Q_q \qquad (A3)$$

$$\partial_p\omega + \nabla\cdot\mathbf{v} = 0 \qquad (A4)$$

where f is the Coriolis parameter, φ the geopotential, $\mathbf{F}_v$ the frictional force, Q_R the radiative heating, and Q_c and Q_q are the convective heat source and moisture sink respectively. Here, $\frac{d}{dt} = \partial_t + \mathbf{v}\cdot\nabla$ is the total derivative following horizontal motion and $\nabla\cdot\mathbf{v}$ is the horizontal divergence.

[45] Within the FT, momentum, temperature, and moisture equations can be expressed, as in QTCM1, as:

$$\mathbf{v}(x,y,p,t) = V_0\mathbf{v}_0(x,y,t) + V_1(p)\mathbf{v}_1(x,y,t) \qquad (A5)$$

$$T(x,y,p,t) = T_r(p) + a_1(p)T_1(x,y,t) \qquad (A6)$$

$$q(x,y,p,t) = q_r(p) + b_1(p)q_1(x,y,t) \qquad (A7)$$

Here, the "barotropic" mode structure function V_0 is independent of pressure in the FT; it is zero-valued in the ABL and is thus not strictly barotropic though the terminology is retained. $V_1(p)$, the profile for the baroclinic mode, is constructed to be consistent with a_1 by hydrostatic balance and is defined with zero mean when integrated over the FT:

$$V_1(p) = a_1^+ - <a_1^+>^F \qquad (A8)$$

where $a_1^+ = \int_{p_t}^{p} a_1(p')d\ln p'$ and the notation $<...>^F$ denotes the vertical average over the FT. Note that the zero mean of $V_1(p)$ over the depth of the FT renders the baroclinic and barotropic modes orthogonal in the FT.

[46] For the implementation of QTCM2, the "bottom" of QTCM1 is lifted and the mixed layer ABL is imposed beneath it. ABL vertical structures for momentum, moisture, and dry static energy are taken as vertically constant within the ABL:

$$\mathbf{v}(x,y,p,t) = \mathbf{v}_b(x,y,t) \qquad (A9)$$

$$s_b(x,y,p,t) = s_{rb} + s_b(x,y,t) \qquad (A10)$$

$$q_b(x,y,p,t) = q_{rb} + q_b(x,y,t) \qquad (A11)$$

For pressure velocity, the vertical structure function $\Omega_1(p)$ is obtained from the continuity equation (A4):

$$\Omega_1(p) = \int_{p_t}^{p_e} V_1(p')dp', \quad p_t < p < p_e, \quad 0 \text{ otherwise} \qquad (A12)$$

The orthogonality of the FT barotropic and baroclinic modes requires $\Omega_1(p_e)=0$ and further necessitates ABL mass convergence (divergence) be balanced by FT barotropic mass divergence (convergence), i.e.,

$$\Delta p_b\nabla\cdot\mathbf{v}_b = -\Delta p_f\nabla\cdot\mathbf{v}_0 = \omega(p_e) \qquad (A13)$$

Thus, the total vertical velocity field is

$$\omega(x,y,p,t) = -\Omega_0\nabla\cdot\mathbf{v}_0 - \Omega_1\nabla\cdot\mathbf{v}_1 \qquad (A14)$$

where $\Omega_0 = \begin{cases} p - p_t & p_t < p < p_e \\ (p_s - p)\Delta p_f/\Delta p_b & p_e < p < p_s \end{cases}$. With the definitions outlined above, the primitive equations can be projected and the vertically-averaged parameters in Table 1 obtained.

References

Back, L. E., and C. S. Bretherton (2009), On the relationship between SST gradients, boundary layer winds and convergence over the tropical oceans, *J. Clim.*, 22, 4182–4196, doi:10.1175/2009JCLI2392.1.

Bellon, G. (2011), Monsoon intraseasonal oscillation and land-atmosphere interaction in an idealized model, *Clim. Dyn.*, 37, 1081–1096, doi:10.1007/s00382-010-0893-0.

Bellon, G., and A. H. Sobel (2008a), Poleward-propagating intraseasonal monsoon disturbances in an intermediate-complexity axisymmetric model, *J. Atmos. Sci.*, 65, 470–489, doi:10.1175/2007JAS2339.1.

Bellon, G., and A. H. Sobel (2008b), Instability of the axisymmetric monsoon flow and intraseasonal oscillation, *J. Geophys. Res.*, 113, D07108, doi:10.1029/2007JD009291.

Bellon, G., and A. H. Sobel (2010), Multiple equilibria of the Hadley circulation in an intermediate-complexity model, *J. Clim.*, 23, 1760–1778, doi:10.1175/2009JCLI3105.1.

Bellon, G., A. H. Sobel, and J. Vialard (2008), Ocean-atmosphere coupling in the monsoon intraseasonal oscillation: A simple model study, *J. Clim.*, 21, 5254–5270, doi:10.1175/2008JCLI2305.1.

Biasutti, M., A. H. Sobel, and Y. Kushnir (2006), GCM precipitation biases in the tropical Atlantic, *J. Clim.*, *19*, 935–958, doi:10.1175/JCLI3673.1.

Betts, A. K., and M. J. Miller (1986), A new convective adjustment scheme. Part II: Single column tests using GATE-wave, BOMEX, ATEX, and Arctic Airmass data sets, *Q. J. R. Meteorol. Soc.*, *112*, 693–709, doi:10.1002/qj.49711247308.

Bretherton, C. S., and A. H. Sobel (2002), A simple model of a convectively coupled Walker circulation using the weak temperature gradient approximation, *J. Clim.*, *15*, 2907–2920, doi:10.1175/1520-0442(2002)015<2907:ASMOAC>2.0.CO;2.

Bretherton, C. S., M. E. Peters, and L. Back (2004), Relationships between water vapor path and precipitation over tropical oceans, *J. Clim.*, *17*, 1517–1528, doi:10.1175/1520-0442(2004)017<1517:RBWVPA>2.0.CO;2.

Burns, S. P., A. H. Sobel, and L. M. Polvani (2006), Asymptotic solutions to the moist axisymmetric Hadley circulation, *Theor. Comput. Fluid Dyn.*, *20*, 443–467, doi:10.1007/s00162-006-0024-z.

Chiang, J. C. H., and A. H. Sobel (2002), Tropical tropospheric temperature variations caused by ENSO and their influence on the remote tropical climate, *J. Clim.*, *15*, 2616–2631, doi:10.1175/1520-0442(2002)015<2616:TTTVCB>2.0.CO;2.

Chou, C., and J. D. Neelin (1996), Linearization of a longwave radiation scheme for intermediate tropical atmospheric models, *J. Geophys. Res.*, *101*, 15,129–15,145, doi:10.1029/96JD01015.

Chou, C., and J. D. Neelin (2003), Mechanisms limiting the northward extent of the northern summer convection zones, *J. Clim.*, *16*, 406–425, doi:10.1175/1520-0442(2003)016<0406:MLTNEO>2.0.CO;2.

Chou, C., and J. D. Neelin (2004), Mechanisms of global warming impacts on regional tropical precipitation, *J. Clim.*, *17*, 2688–2701, doi:10.1175/1520-0442(2004)017<2688:MOGWIO>2.0.CO;2.

Cuijpers, H., and P. Bechtold (1995), A simple parameterization of cloud water related variables for use in boundary layer models, *J. Atmos. Sci.*, *52*, 2486–2490, doi:10.1175/1520-0469(1995)052<2486:ASPOCW>2.0.CO;2.

Dai, A. (2006), Precipitation characteristics in eighteen coupled climate models, *J. Clim.*, *19*, 4605–4630, doi:10.1175/JCLI3884.1.

Del Genio, A. D. (2012), Representing the sensitivity of convective cloud systems to tropospheric humidity in general circulation models, *Surv. Geophys.*, *33*, 637–656, doi:10.1007/s10712-011-9148-9.

Derbyshire, S. H., I. Beau, P. Bechtold, J.-Y. Grandpeix, J.-M. Piriou, J.-L. Redelsperger, and P. M. M. Soares (2004), Sensitivity of moist convection to environmental humidity, *Q. J. R. Meteorol. Soc.*, *130*, 3055–3079, doi:10.1256/qj.03.130.

Frierson, D. M. (2007), Convectively coupled Kelvin waves in an idealized moist general circulation model, *J. Atmos. Sci.*, *64*, 2076–2090, doi:10.1175/JAS3945.1.

Grabowski, W. W. (2006), Impact of explicit atmosphere–ocean coupling on MJO-like coherent structures in idealized aquaplanet simulations, *J. Atmos. Sci.*, *63*, 2289–2306, doi:10.1175/JAS3740.1.

Grabowski, W. W., and M. W. Moncrieff (2004), Moisture-convection feedback in the tropics, *Q. J. R. Meteorol. Soc.*, *130*, 3081–3104, doi:10.1256/qj.03.135.

Hannah, W. M., and E. D. Maloney (2011), The role of moisture–convection feedbacks in simulating the Madden–Julian Oscillation, *J. Clim.*, *24*, 2754–2770, doi:10.1175/2011JCLI3803.1.

Holloway, C. E., and J. D. Neelin (2007), The convective cold top and quasi equilibrium, *J. Atmos. Sci.*, *64*, 1467–1487, doi:10.1175/JAS3907.1.

Holloway, C. E., and J. D. Neelin (2009), Moisture vertical structure, column water vapor, and tropical deep convection, *J. Atmos. Sci.*, *66*, 1665–1683, doi:10.1175/2008JAS2806.1.

Holloway, C. E., and J. D. Neelin (2010), Temporal relations of column water vapor and tropical precipitation, *J. Atmos. Sci.*, *67*, 1091–1105, doi:10.1175/2009JAS3284.1.

Jackson, C. S., M. K. Sen, G. Huerta, Y. Deng, and K. P. Bowman (2008), Error reduction and convergence in climate prediction, *J. Clim.*, *21*, 6698–6709, doi:10.1175/2008JCLI2112.1.

Kanamitsu, M., W. Ebisuzaki, J. Woollen, S.-K. Yang, J. J. Hnilo, M. Fiorino, and G. L. Potter (2002), NCEP-DEO AMIP-II reanalysis (R-2), *Bull. Am. Meteorol. Soc.*, *83*, 1631–1643, doi:10.1175/BAMS-83-11-1631.

Khouider, B., and A. J. Majda (2006), A simple multicloud parameterization for convectively coupled tropical waves. Part I: Linear analysis, *J. Atmos. Sci.*, *63*, 1308–1323, doi:10.1175/JAS3677.1.

Kim, D., A. H. Sobel, E. D. Maloney, D. M. W. Frierson, and I.-S. Kang (2011), A Systematic relationship between intraseasonal variability and mean state bias in AGCM simulations, *J. Clim.*, *24*, 5506–5520, doi:10.1175/2011JCLI4177.1.

Kuang, Z., and C. S. Bretherton (2006), A mass flux scheme view of a high-resolution simulation of a transition from shallow to deep cumulus convection, *J. Atmos. Sci.*, *63*, 1895–1909, doi:10.1175/JAS3723.1.

Lin, J. W., J. D. Neelin, and N. Zeng (2000), Maintenance of tropical intraseasonal variability: Impact of evaporation-wind feedback and midlatitude storms, *J. Atmos. Sci.*, *57*, 2793–2823, doi:10.1175/1520-0469(2000)057<2793:MOTIVI>2.0.CO;2.

Lindzen, R. S., and S. Nigam (1987), On the role of sea surface temperature gradients in forcing low-level winds and convergence in the tropics, *J. Atmos. Sci.*, *44*, 2418–2436, doi:10.1175/1520-0469(1987)044<2418:OTROSS>2.0.CO;2.

Lintner, B. R., and J. C. H. Chiang (2007), Adjustment of the remote tropical climate to El Niño conditions, *J. Clim.*, *20*, 2544–2557, doi:10.1175/JCLI4138.1.

Lintner, B. R., and J. D. Neelin (2007), A prototype for convective margin shifts, *Geophys. Res. Lett.*, *34*, L05812, doi:10.1029/2006GL027305.

Lintner, B. R., and J. D. Neelin (2008), Eastern margin variability of the South Pacific Convergence Zone, *Geophys. Res. Lett.*, *35*, L16701, doi:10.1029/2008GL034298.

Lintner, B. R., P. Gentine, K. L. Findell, F. D'Andrea, A. H. Sobel, and G. D. Salvucci (2012), An idealized prototype for large-scale land-atmosphere coupling, *J. Clim.*, doi:10.1175/JCLI-D-11-00561.1, in press.

Neelin, J. D., and H. Su (2005), Moist teleconnection mechanisms for the tropical South American and Atlantic sector, *J. Clim.*, *18*, 3928–3950, doi:10.1175/JCLI3517.1.

Neelin, J. D., and N. Zeng (2000), A quasi-equilibrium tropical circulation model—Formulation, *J. Atmos. Sci.*, *57*, 1741–1766, doi:10.1175/1520-0469(2000)057<1741:AQETCM>2.0.CO;2.

Neelin, J. D., C. Chou, and H. Su (2003), Tropical drought regions in global warming and El Niño teleconnections, *Geophys. Res. Lett.*, *30*(24), 2275, doi:10.1029/2003GL018625.

Neggers, R., B. Stevens, and J. D. Neelin (2006), A simple equilibrium model for shallow cumulus convection, *Theor. Comput. Fluid Dyn.*, *20*, 305–322, doi:10.1007/s00162-006-0030-1.

Neggers, R. A. J., J. D. Neelin, and B. Stevens (2007), Impact mechanisms of shallow cumulus convection on tropical climate dynamics, *J. Clim.*, *20*, 2623–2642, doi:10.1175/JCLI4079.1.

Oueslati, B., and G. Bellon (2012), Tropical precipitation regimes and mechanisms of regime transitions: Contrasting two aquaplanet general circulation models, *Clim. Dyn.*, doi:10.1007/s00382-012-1344-x, in press.

Parsons, D. B., K. Yoneyama, and J.-L. Reddelsperger (2000), The evolution of the tropical western Pacific atmosphere-ocean system following the arrival of a dry intrusion, *Q. J. R. Meteorol. Soc.*, *126*, 517–548, doi:10.1002/qj.49712656307.

Sahany, S., J. D. Neelin, K. Hales, and R. Neale (2012), Temperature-moisture dependence of the deep convective transition as a constraint on entrainment in climate models, *J. Atmos. Sci.*, *69*, 1340–1358, doi:10.1175/JAS-D-11-0164.1.

Sherwood, S. C., P. Minnis, and M. McGill (2004), Deep convective cloud top heights and their thermodynamic control during CRYSTAL-FACE, *J. Geophys. Res.*, *109*, D20119, doi:10.1029/2004JD004811.

Sobel, A. H. (2007), Simple models of ensemble-averaged precipitation and surface wind, given the sea surface temperature, in *The Global Circulation of the Atmosphere*, edited by T. Schneider and A. H. Sobel, pp. 219–251, Princeton Univ. Press, Princeton, N. J.

Sobel, A. H., and C. S. Bretherton (2000), Modeling tropical precipitation in a single column, *J. Clim.*, *13*, 4378–4392, doi:10.1175/1520-0442(2000)013<4378:MTPIAS>2.0.CO;2.

Sobel, A. H., and J. D. Neelin (2006), The boundary layer contribution to intertropical convergence zones in the quasi-equilibrium tropical circulation model framework, *Theor. Comput. Fluid Dyn.*, *20*, 323–350, doi:10.1007/s00162-006-0033-y.

Sobel, A. H., J. Nilsson, and L. M. Polvani (2001), The weak temperature gradient approximation and balanced tropical moisture waves, *J. Atmos. Sci.*, *58*, 3650–3665, doi:10.1175/1520-0469(2001)058<3650:TWTGAA>2.0.CO;2.

Sobel, A. H., C. S. Bretherton, H. Gildor, and M. E. Peters (2004), Convection, cloud-radiative feedbacks and thermodynamic ocean coupling in simple models of the Walker circulation, in *Earth's Climate: The Ocean-Atmosphere Interaction, Geophys. Monogr. Ser.*, vol. 147, edited by C. Wang, S.-P. Xie, and J. A. Carton, pp. 393–405, AGU, Washington, D. C, doi:10.1029/147GM22.

Su, H., and J. D. Neelin (2005), Dynamical mechanisms for African monsoon changes during the mid-Holocene, *J. Geophys. Res.*, *110*, D19105, doi:10.1029/2005JD005806.

Tompkins, A. M. (2001), Organization of tropical convection in low vertical wind shears: The role of water vapor, *J. Atmos. Sci.*, *58*, 529–545, doi:10.1175/1520-0469(2001)058<0529:OOTCIL>2.0. CO;2.

Xie, P., and P. A. Arkin (1997), Global precipitation: A 17-year monthly analysis based on gauge observations, satellite estimates, and numerical model outputs, *Bull. Am. Meteorol. Soc.*, *78*, 2539–2558, doi:10.1175/1520-0477(1997)078<2539:GPAYMA>2. 0.CO;2.

Zeng, N., J. D. Neelin, and C. Chou (2000), A quasi-equilibrium tropical circulation model–Implementation and simulation, *J. Atmos. Sci.*, *57*, 1767–1796, doi:10.1175/1520-0469(2000)057<1767: AQETCM>2.0.CO;2.

Corresponding author: B. R. Lintner, Department of Environmental Sciences, Rutgers, State University of New Jersey, 14 College Farm Rd., New Brunswick, NJ 08901-8551, USA. (lintner@envsci.rutgers.edu)